J|A|C|S ARTICLES

Published on Web 06/03/2010

Simulation of Electrocatalytic Hydrogen Production by a Bioinspired Catalyst Anchored to a Pyrite Electrode

Federico Zipoli,*,† Roberto Car,†,‡ Morrel H. Cohen,†,§ and Annabella Selloni*,†

Department of Chemistry, Princeton Institute for the Science and Technology of Materials, Princeton University, Princeton, New Jersey 08544, and Department of Physics and Astronomy, Rutgers University, Piscataway, New Jersey 08854

Received December 18, 2009; E-mail: fzipoli@princeton.edu; aselloni@princeton.edu

Abstract: The possibility of using the active site, the $[FeFe]_H$ cluster, of the bacterial di-iron hydrogenases as a catalyst for hydrogen production from water by electro- or photocatalysis is of current scientific and technological interest. We present here a theoretical study of hydrogen production by a modified $[FeFe]_H$ cluster stably linked to a pyrite electrode immersed in acidified water. We employed state-of-the-art electronic-structure and first-principles molecular-dynamics methods. We found that a stable sulfur link of the cluster to the surface analogous to that linking the cluster to its enzyme environment cannot be made. However, we have discovered a modification of the cluster which does form a stable, tridentate link to the surface. The pyrite electrode readily produces hydrogen from acidified water when functionalized with the modified cluster, which remains stable throughout the hydrogen production cycle.

1. Introduction

The hydrogen evolution reaction

$$H_2 \leftrightarrow 2H^+ + 2e^- \quad (1)$$

is a central process in the global biological energy cycle. It is mediated by three different classes of enzymes with multiple subgroups.[1,2] Of these, the di-iron hydrogenases, normally found in H_2-producing microorganisms, show the highest turnover frequency, over 9000 H_2 molecules per second at room temperature, 1 or 2 orders of magnitude higher than that typical of [NiFe] hydrogenases. The catalytic properties of these enzymes have been extensively studied both theoretically[3−13] and experimentally.[14−24] In particular, both the [FeFe]-[25,26] and [NiFe]-enzymes[22,26] have been linked to electrodes and shown to generate H_2; for instance, it was shown that the [NiFeSe]-hydrogenase linked to a dye-sensitized TiO_2 photoelectrode can generate H_2 from neutral water and visible light at room temperature.[22] However, there are disadvantages to using enzymes.[14] First, these enzymes are large molecules. Each enzyme would occupy a surface area of about 100 nm^2, which imposes a strong limit on the number of active sites per unit

† Department of Chemistrys, Princeton University.
‡ Princeton Institute for the Science and Technology of Materials, Princeton University.
§ Department of Physics and Astronomy, Rutgers University.

(1) Vignais, P. M.; Billoud, B.; Meyer, J. *Fems Microbiol. Rev.* **2001**, *25*, 455–501.
(2) Fontecilla-Camps, J. C.; Volbeda, A.; Cavazza, C.; Nicolet, Y. *Chem. Rev.* **2007**, *107*, 4273–4303.
(3) Bruschi, M.; Greco, C.; Kaukonen, M.; Fantucci, P.; Ryde, U.; De Gioia, L. *Angew. Chem., Int. Ed.* **2009**, *48*, 3503–3506.
(4) Cao, Z. X.; Hall, M. B. *J. Am. Chem. Soc.* **2001**, *123*, 3734–3742.
(5) Liu, Z. P.; Hu, P. *J. Am. Chem. Soc.* **2002**, *124*, 5175–5182.
(6) Bruschi, M.; Fantucci, P.; De Gioia, L. *Inorg. Chem.* **2002**, *41*, 1421–1429.
(7) Greco, C.; Bruschi, M.; De Gioia, L.; Ryde, U. *Inorg. Chem.* **2007**, *46*, 5911–5921.
(8) Fiedler, A. T.; Brunold, T. C. *Inorg. Chem.* **2005**, *44*, 9322–9334.
(9) Zilberman, S.; Stiefel, E. I.; Cohen, M. H.; Car, R. *J. Phys. Chem. B* **2006**, *110*, 7049–7057.
(10) Szilagyi, R. K.; Winslow, M. A. *J. Comput. Chem.* **2006**, *27*, 1385–1397.
(11) Liu, T. B.; Li, B.; Singleton, M. L.; Hall, M. B.; Darensbourg, M. Y. *J. Am. Chem. Soc.* **2009**, *131*, 8296–8307.
(12) Siegbahn, P. E. M.; Tye, J. W.; Hall, M. B. *Chem. Rev.* **2007**, *107*, 4414–4435.
(13) Fan, H. J.; Hall, M. B. *J. Am. Chem. Soc.* **2001**, *123*, 3828–3829.
(14) Cracknell, J. A.; Vincent, K. A.; Armstrong, F. A. *Chem. Rev.* **2008**, *108*, 2439–2461.
(15) Tye, J. W.; Hall, M. B.; Darensbourg, M. Y. *Proc. Natl. Acad. Sci. U.S.A.* **2005**, *102*, 16911–16912.
(16) Tard, C.; Liu, X. M.; Ibrahim, S. K.; Bruschi, M.; De Gioia, L.; Davies, S. C.; Yang, X.; Wang, L. S.; Sawers, G.; Pickett, C. J. *Nature* **2005**, *433*, 610–613.
(17) Peters, J. W.; Lanzilotta, W. N.; Lemon, B. J.; Seefeldt, L. C. *Science* **1998**, *282*, 1853–1858.
(18) Nicolet, Y.; de Lacey, A. L.; Vernede, X.; Fernandez, V. M.; Hatchikian, E. C.; Fontecilla-Camps, J. C. *J. Am. Chem. Soc.* **2001**, *123*, 1596–1601.
(19) Vincent, K. A.; Cracknell, J. A.; Lenz, O.; Zebger, I.; Friedrich, B.; Armstrong, F. A. *Proc. Natl. Acad. Sci. U.S.A.* **2005**, *102*, 16951–16954.
(20) Nicolet, Y.; Piras, C.; Legrand, P.; Hatchikian, C. E.; Fontecilla-Camps, J. C. *Structure Folding Design* **1999**, *7*, 13–23.
(21) Lubitz, W.; Reijerse, E.; van Gastel, M. *Chem. Rev.* **2007**, *107*, 4331–4365.
(22) Reisner, E.; Fontecilla-Camps, J. C.; Armstrong, F. A. *Chem. Commun.* **2009**, 550–552.
(23) Felton, G. A. N.; Vannucci, A. K.; Chen, J. Z.; Lockett, L. T.; Okumura, N.; Petro, B. J.; Zakai, U. I.; Evans, D. H.; Glass, R. S.; Lichtenberger, D. L. *J. Am. Chem. Soc.* **2007**, *129*, 12521–12530.
(24) Felton, G. A. N.; Vannucci, A. K.; Okumura, N.; Lockett, L. T.; Evans, D. H.; Glass, R. S.; Lichtenberger, D. L. *Organometallics* **2008**, *27*, 4671–4679.
(25) Hambourger, M.; Gervaldo, M.; Svedruzic, D.; King, P. W.; Gust, D.; Ghirardi, M.; Moore, A. L.; Moore, T. A. *J. Am. Chem. Soc.* **2008**, *130*, 2015–2022.
(26) Lubner, C. E.; Grimme, R.; Bryant, D. A.; Golbeck, J. H. *Biochemistry* **2010**, *49*, 404–414.

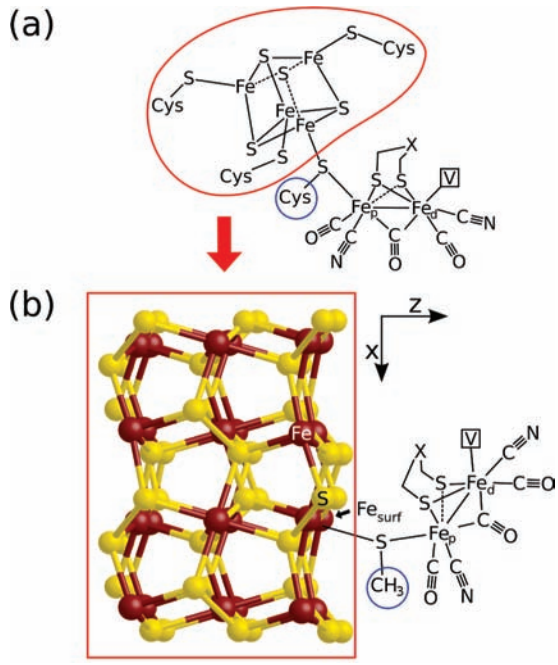

Figure 1. (a) Sketch of the active center, the $[FeFe]_H$ cluster of the diiron hydrogenases. It is connected to an Fe_4S_4 cubane and to a cysteine in the enzyme's backbone by a thiol link. (b) Sketch of the active center linked to an Fe atom on the FeS_2 (100) surface. The Fe_4S_4 cubane (red contour in (a)) has been replaced by the pyrite surface, the electrode (red rectangle in (b)), and the thiol−cysteine (blue circle in (a)) link to the $[FeFe]_H$ cluster has been replaced by an SCH_3 (blue circle in (b)), terminating the cluster. The distal iron (Fe_d) has a vacant site, indicated by V, cf. Figure 2. The pyrite (100) surface is modeled by a slab nine atomic layers thick. The atoms of the slab are indicated with balls and sticks; Fe atoms are dark red, and S atoms are yellow. **z** indicates the normal to the surface.

area of the surface. Consequently a monolayer of enzyme cannot provide useful currents for most purposes.[27] Structured multilayers of enzymes, designed to ensure mass transport, can only partially overcome this limitation.[27] Second, during the enzyme's biological activity, electron transfer to the active site from a docked ferrotin occurs through an intermediate chain of Fe−S clusters (the electron channel). Presumably, an analogous process occurs when the enzyme is on an electrode. Avoiding this need to shuttle the electrons would be beneficial. In view of these concerns, the possibility of H_2 production by the naked active center, detached from the enzyme and directly linked to the electrode, is particularly interesting. An illustrative sketch is shown in Figure 1. It would ensure a two-order-of-magnitude higher surface density of active centers and fast electron transfer due to efficient active center to electrode coupling.

Within the active site of the enzyme (Figure 1), there is a diiron cluster, $[FeFe]_H$, which is linked to the terminal Fe_4S_4 cubane of the electron channel at its proximal iron, Fe_p, via a cysteine within the protein backbone. The remaining iron, Fe_d, is distal to that link. In addition to the electron channel, this active center is exposed to another channel through which protons are supplied.[19]

In commonly studied models of the $[FeFe]_H$ cluster, cf. Figure 2, the cubane−cysteine−thiol link is replaced by a methylthiol. As in the enzyme, the Fe_p and Fe_d atoms are coordinated with CO and CN ligands and bridged by a chelating group, SCH_2XCH_2S where X can, e.g., be an NH (DTMA) or CH_2

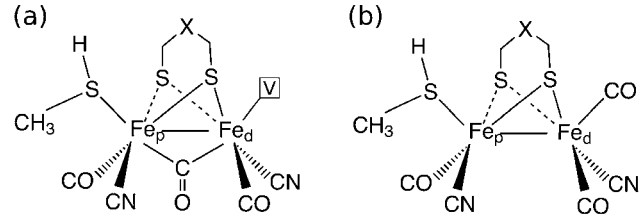

Figure 2. Sketches of the active center of the diiron hydrogenases, $[FeFe]_H$, terminated by SCH_3 in its bridging (a) and terminal (b) configurations. In (a), the configuration in the enzyme, the distal iron has a vacant site, indicated by V, which can coordinate ligands such as CO, H_2O, etc.... The "X" in the chelating SCH_2XCH_2S group stands for CH_2, NH, or O.[18]

(PDT) group.[20] Two important groups of isomers have been identified,[4,28] CO-bridging (μ-CO, Figure 2a) and CO-terminal (CO_T, Figure 2b). They differ in the position of one of the CO ligands. In CO_T each CO is connected to only one of the two iron atoms, while in μ-CO there is one CO, the μ-CO, bridging the two iron atoms and leaving a vacant coordination site V on Fe_d. μ-CO is the configuration of the active, ready state of the enzyme;[18] hydrogen production occurs at V. In previous work,[29] we showed that the CO-bridging configuration had to be stable for the $[FeFe]_H$ cluster of hydrogenase to function as an efficient hydrogen-production catalyst. We found that in vacuo, however, the CO-terminal configuration was slightly more stable and would effectively stop catalytic action. Since in practical applications the cluster would be immersed in acidified water, we subsequently studied[30] the effects of a water environment on its structure and reactivity. The electrons for the reaction (**1**) were added without considering the electrode explicitly, an artifice eliminated in the present work. The main advantages of the model used in ref 30 were that the electrostatic effects, the dynamics of the proton diffusion in water via the Grotthuss-shuttle mechanism, and the proton sharing between the cluster and the water molecules were all taken into account in the First Principles Molecular Dynamic (FPMD) computations. The main results were as follows: (i) interconversion between the bridging and terminal configurations occurs without significant activation energies; (ii) the presence of terminal isomers does not stop the catalytic activity because a local hydrophobicity kinetically prevents the formation of a low energy CO_T isomer in which a proton bridges the two Fe atoms (μ-H); (iii) with a DTMA chelating group, there are at least three different pathways for H_2 production by the bridging configuration which involve a sequential protonation of Fe_d only or of both Fe_d and DTMA; and (iv) the bare active center of the diiron hydrogenases can be an efficient catalyst for H_2 production provided that electrons are transferred to the cluster. However, we also found (v) that when the cluster is detached from the enzyme and immersed in acidified water, there are configurations in which the bond between Fe_p and the S modeling the linking thiol is weak and can break. The stability of the link between the electrode and the di-iron cluster was thus found to be a key issue in the design of a viable system.

In the present work, we replace the electron channel of the enzyme by an FeS_2 (pyrite) electrode as the source of electrons for **1**. The link to the cubane and the cysteine of the enzyme is replaced by a tridentate linkage to the (100) surface of the pyrite.

(27) Barton, S. C.; Gallaway, J.; Atanassov, P. *Chem. Rev.* **2004**, *104*, 4867–4886.
(28) Liu, Z. P.; Hu, P. *J. Am. Chem. Soc.* **2002**, *124*, 11568–11569.
(29) Sbraccia, C.; Zipoli, F.; Car, R.; Cohen, M. H.; Dismukes, G. C.; Selloni, A. *J. Phys. Chem. B* **2008**, *112*, 13381–13390.
(30) Zipoli, F.; Car, R.; Cohen, M. H.; Selloni, A. *J. Phys. Chem. B* **2009**, *113*, 13096–13106.

The latter was chosen as an electrode because of its resemblance to the cubane and its compatibility with the Fe_2S_2 moiety of the $[FeFe]_H$ cluster. The functionalized surface is immersed in acidified water as a source of protons for **1**.

To function successfully in the environment defined by the pyrite surface and the acidified water, so different from that within the enzyme, the $[FeFe]_H$ cluster must be modified so as to meet four requirements:

(a) The cluster-pyrite linkage must be stable.

(b) There must be a vacant coordination site V on Fe_d; V must be exposed to the aqueous environment.

(c) The cluster itself must be stable throughout the H_2 production cycle.

(d) The modifications of the cluster needed for requirements a−c must not interfere with its H_2 production capacity.

We report elsewhere[31] the steps of a successful search for modifications which meet all four requirements. The search was carried out by modeling the functionalized surface and investigating its stability and catalytic properties via static density-functional-theory (DFT) computations and first-principles molecular-dynamics simulations.[26] In the present paper, we present a study of simulated hydrogen production by the resulting cluster/pyrite system.

A modified $[FeFe]_H$ cluster which meets these four requirements is shown in Figure 3. The modifications include the following: (1) elimination of the methylthiol of Figure 2 used in refs 29 and 30 and by other workers[4−9] to model the linkage of Fe_p to the cubane; (2) hydrogenating the CN ligands on Fe_p and Fe_d; (3) interchanging the CO and CNH ligands on Fe_p for requirement a; (4) interchanging the μ-CO and the CNH ligands on Fe_d for requirements a and b; (5) choosing PDT (for which $X = CH_2$) as the chelating group for requirement c; and (6) substitution of a P−H group for that S of the chelating group which would be exposed to water, especially important for requirement c. We shall use the symbol $[FeFe]_P$ for the modified cluster *bound to the surface* to emphasize the importance of the phosphorus substitution for the performance of the catalyst.

2. Methods

Our study employs Car−Parrinello (CP)[32] FPMD simulations of the $[FeFe]_H$ cluster in a liquid-water environment with or without hydronium ions. The FPMD simulations were performed within the framework of density-functional theory in the local-spin-density approximation supplemented by generalized-gradient corrections,[33] as implemented in the CP code of the Quantum-ESPRESSO package.[34] We employed ultrasoft pseudopotentials[35,36] with a plane-wave expansion of the Kohn−Sham orbitals (of the augmented density) up to a kinetic energy cutoff of 30 Ry (of 240 Ry). The pyrite (100) surface was modeled in a slab geometry with 3D periodic boundary conditions at the experimental lattice parameter, 5.428 Å.[37] (Our theoretical lattice constant, computed with fully converged Brillouin zone (BZ) sampling, is 5.404 Å, i.e., only 0.4% shorter than the experimental one.) We considered a 2×2 supercell having the ideal termination of the bulk. The slab was nine atomic layers thick (24 FeS_2 units, cf. Figure 1). For calculations in vacuo, adjacent slabs were separated by 15 Å in a tetragonal simulation box with $a = 10.856$ Å and $c = 21.712$ Å. The atoms of the three bottom layers were fixed to their positions in the clean surface during geometry optimizations of the supported catalyst, whereas all atoms were free to move during the FPMD simulations. We used only the Γ point to sample the surface BZ for both FPMD and structural optimizations. Test calculations comparing the results of the Γ-point integration with those of a *k*-point mesh showed differences in relative energies of the order of k_BT. We attached the diiron $[FeFe]_P$ cluster (see section 3 and Figure 3) to the FeS_2(100) surface, increased *c* to 32.568 Å, and added 79 water molecules to simulate immersion of the supported

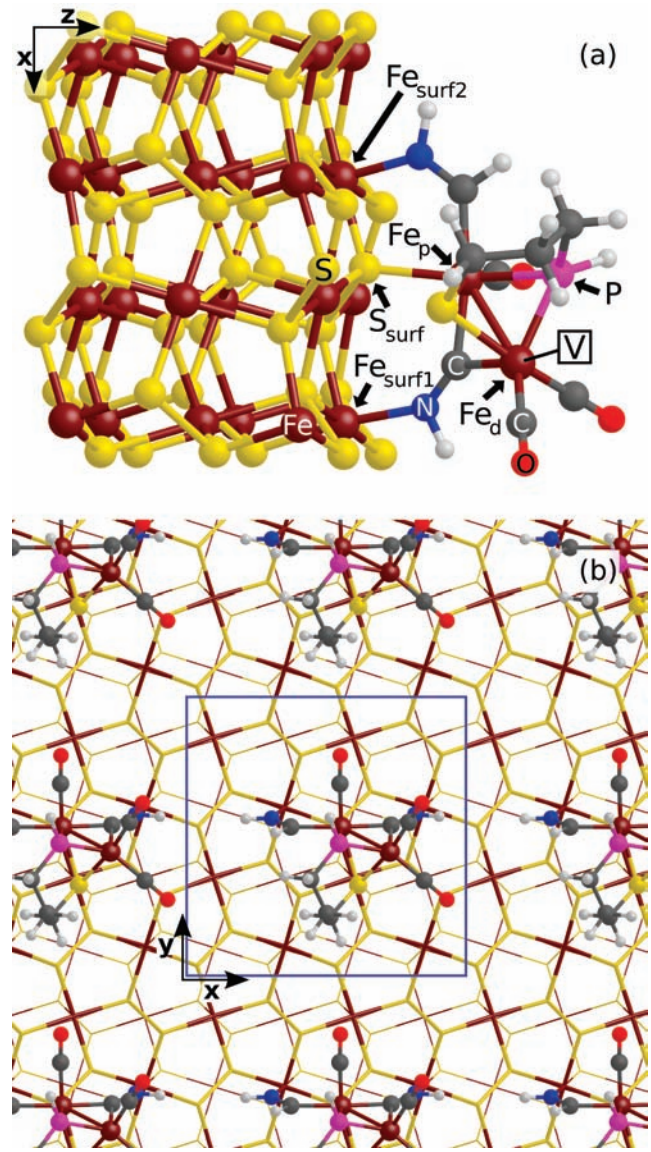

Figure 3. Side (a) and top (b) views of the $[FeFe]_P$ cluster linked to an S-atom (S_{surf}) on the FeS_2 (100) surface via a direct Fe_p-S_{surf} bond. In (b), the geometry has been replicated in the (*x*,*y*) plane; the box is represented by the continuous blue line. The distal and the proximal irons are indicated by the labels Fe_d and Fe_p, respectively. Fe_p and Fe_d are bridged by an $SCH_2CH_2CH_2P$ group. A $(CN)_dH$ group bridges the Fe_p and Fe_d and is connected to an Fe atom of the surface (Fe_{surf1}) via a dative bond between N and Fe_{surf1}. The distal iron has a vacant site, indicated by V. A second dative bond forms between a second surface iron (Fe_{surf2}) and the N atom of $(CHNH)_p$. Fe atoms are dark red; S atoms are yellow; the P atom is pink; C atoms are dark gray; N atoms are blue; O atoms are red; and H atoms are shaded. In (b), the atoms of the slab are represented with sticks only.

(31) Zipoli, F.; Car, R.; Cohen, M. H.; Selloni, A. To be published.
(32) Car, R.; Parrinello, M. *Phys. Rev. Lett.* **1985**, *55*, 2471–2474.
(33) Perdew, J. P.; Burke, K.; Ernzerhof, M. *Phys. Rev. Lett.* **1997**, *78*, 1396–1396.
(34) Giannozzi, P.; et al. *J. Phys.: Condens. Matter* **2009**, *21*, 395502–395520.
(35) Vanderbilt, D. *Phys. Rev. B* **1990**, *41*, 7892–7895.
(36) Laasonen, K.; Pasquarello, A.; Car, R.; Lee, C.; Vanderblit, D. *Phys. Rev. B* **1993**, *47*, 10142–10153.
(37) Finklea, S. L.; Cathey, L.; Amma, E. L. *Acta Crystallogr., Sect. A* **1976**, *32*, 529–537.

cluster in water of real density for the computations reported here. A fictitious electronic mass of 350 au and a time step of 0.072 fs were used in the FPMD simulations. Constant temperature was imposed on the ions by a massive Nosé−Hoover thermostat.[38,39] In situations where the system's HOMO−LUMO energy gap was "small" (less than 0.1 eV), adiabaticity of the FPMD trajectory was maintained by coupling two separate Nosé−Hoover thermostats to the nuclear and electronic subsystems.[40] Static calculations on the supported $[FeFe]_P$ cluster in vacuo were performed using the PW code of the Quantum-ESPRESSO package.[34] Energy barriers were calculated using the climbing-image nudged-elastic-band (NEB)[41] and the string[42] methods. For geometry optimizations and energy-barrier determinations, the norm of the force vector was required to be smaller than 5 meV/Å at convergence. Free energy barriers were calculated using thermodynamic integration[43] with the reaction coordinate used by Leung et al.,[44] cf. section 4.2. Different pseudopotentials were used for the iron atoms of the cluster and for those of the pyrite slab, with 16 and 8 electrons explicitly treated as valence electrons, respectively. This choice reduced the computational cost without affecting the accuracy of our description of the delicate chemistry involving the two iron atoms of the $[FeFe]_P$ cluster. The validity of DFT for addressing the electronic and chemical properties of the FeS_2 surface[45−48] and the $[FeFe]_H$ cluster of the diiron hydrogenase in different environments has been widely established.[3−12,29,30] Because the duration of our simulations is limited to a few picoseconds, each computed trajectory may remain sensitive to the initial conditions imposed. To overcome this possible source of bias, we normally compute several trajectories spanning a representative range of initial conditions.

3. Model

FeS_2(100) Surface. The stoichiometric (100) surface of pyrite is formed by breaking the Fe−S bonds between adjacent (100) atomic layer planes while keeping intact the sulfur−dimer units. The S and Fe atoms on the FeS_2 surface(bulk) are 3(4)- and 5(6)-fold coordinated, respectively. The LUMO of the clean defect-free surface derives from the d_z^2 orbitals of the surface iron atoms, and the computed band gap is 0.50 eV (0.42 eV for bulk pyrite, compared to the experimental value of ∼0.9 eV,[49] a typical DFT underestimate). This inaccuracy, however, is not important for the present study, where the (adiabatic) ground-state electronic structure is always considered.

Water adsorption on the FeS_2 (100) surface has been extensively studied both theoretically[45,48,50−52] and experimentally;[53,54] see refs 55 and 56 and references therein. In agreement with these previous studies, we found that water adsorbs in molecular form via a coordinative covalent bond between a lone-pair orbital of its oxygen and an empty d_z^2 orbital of a surface iron atom. The computed adsorption energy is 13.1 kcal/mol at low (1/8 ML) coverage. Due to intermolecular H-bond formation, this binding energy increases slightly with increasing coverage and becomes 14.3 kcal/mol at full (1 ML) coverage.

Supported Catalyst. Our initial hypothesis for the supported catalyst is sketched in Figure 1b. In order to satisfy all four requirements stated in the Introduction, we found several modifications of the composition and structure of the cluster to be necessary. The conceptual path we followed to get to the final form of the catalyst is interesting; it offers chemical and physical insights into this complex system, which could in principle be used to guide experimentalists through the synthesis of a stable and active catalyst. However, since our main focus here is on the demonstration of stable hydrogen production, we present results only for the final catalyst candidate. A detailed description of the path to the modifications will be presented in a forthcoming publication;[31] a brief summary follows.

In analogy to the link between the $[FeFe]_H$ cluster and the cubane in the enzyme, one could imagine attaching the catalyst to the pyrite surface by using the sulfur atom (S) of an SCH_3 to connect the Fe_p to one of the surface Fe atoms (Fe_{surf1}), as in Figure 1b. In ref 30, we pointed out that the Fe_p-SCH_3 link is weak in the absence of the electrode. In particular, we found that when the active center is removed from the pocket of the enzyme and immersed in acidified water, there are five sites on the $[FeFe]_H$ cluster which can be easily protonated/deprotonated. Protonation of one of those sites, the S atom of SCH_3, weakens the Fe_p−thiol bond, which can subsequently break. We concluded that the link with the electrode should *not* be made with a bridging sulfur even though the corresponding link is stable in the enzyme. To overcome this problem, we removed the bridging thiol to allow a direct bond between Fe_p and a sulfur atom on the FeS_2 (100) surface, S_{surf} (cf. Figure 3a). Here, the CN groups connected to both Fe_p and Fe_d, $(CN)_p$ and $(CN)_d$, were protonated, as usually found in acidified water.[30] The Fe_p-S_{surf} link restores the 4-fold coordination that sulfur atoms have in the pyrite bulk. In ref 30, we reported observing during an FPMD simulation at $T = 300-350$ K in water an unusual structure with a $(CN)_d$-H group bridging the two iron atoms, cf. Figure 6d of ref 30. The spontaneous formation of this unusual isomer suggests that its energy is close to those of μ-CO and CO_T. Accordingly, the diiron cluster of Figure 3 has a $(CN)_d$-H group bridging the Fe_p and Fe_d, μ-$(CN)_d$-H, instead of a CO group. We chose this previously observed isomer because we wanted to use the dative bond between the N atom of $(CN)_d$-H and a surface iron atom (Fe_{surf1} in Figure 3a) to lock the system into the bridging configuration with the vacant site on Fe_d exposed to H_2O. We subsequently found that a third bond with the surface can form between the N atom of $(CN)_p$ and a second iron atom on the surface, Fe_{surf2} in Figure 3a, resulting in a stable tridentate linkage of the cluster to the electrode.

(38) Martyna, G. J.; Klein, M. L.; Tuckerman, M. *J. Chem. Phys.* **1992**, *97*, 2635–2643.
(39) Nosé, S. *Prog. Theor. Phys. Suppl.* **1991**, 1–46.
(40) Blöchl, P. E.; Parrinello, M. *Phys. Rev. B* **1992**, *45*, 9413–9416.
(41) Henkelman, G.; Uberuaga, B. P.; Jónsson, H. *J. Chem. Phys.* **2000**, *113*, 9901–9904.
(42) E, W. N.; Ren, W. Q.; Vanden-Eijnden, E. *Phys. Rev. B* **2002**, *66*, 052301−052304.
(43) Kirkwood, J. G. *J. Chem. Phys.* **1935**, *3*, 300–313.
(44) Leung, K.; Nielsen, I. M. B.; Criscenti, L. J. *J. Am. Chem. Soc.* **2009**, *131*, 18358–18365.
(45) Nair, N. N.; Schreiner, E.; Marx, D. *J. Am. Chem. Soc.* **2006**, *128*, 13815–13826.
(46) Stirling, A.; Bernasconi, M.; Parrinello, M. *Phys. Rev. B* **2007**, *75*, 165406–165413.
(47) Stirling, A.; Bernasconi, M.; Parrinello, M. *J. Chem. Phys.* **2003**, *119*, 4934–4939.
(48) Stirling, A.; Bernasconi, M.; Parrinello, M. *J. Chem. Phys.* **2003**, *118*, 8917–8926.
(49) Ferrer, I. J.; Nevskaia, D. M.; Delasheras, C.; Sánchez, C. *Solid State Commun.* **1990**, *74*, 913–916.
(50) Schreiner, E.; Nair, N. N.; Marx, D. *J. Am. Chem. Soc.* **2008**, *130*, 2768–2770.
(51) Boehme, C.; Marx, D. *J. Am. Chem. Soc.* **2003**, *125*, 13362–13363.
(52) Rodriguez, J. A.; Abreu, I. A. *J. Phys. Chem. B* **2005**, *109*, 2754–2762.
(53) Kendelewicz, T.; Doyle, C. S.; Bostick, B. C.; Brown, G. E. *Surf. Sci.* **2004**, *558*, 80–88.
(54) Rosso, K. M.; Becker, U.; Hochella, M. F. *Am. Mineral.* **1999**, *84*, 1549–1561.
(55) Rickard, D.; Luther, G. W. *Chem. Rev.* **2007**, *107*, 514–562.
(56) Murphy, R.; Strongin, D. R. *Surf. Sci. Rep.* **2009**, *64*, 1–45.

Table 1. Relevant Bond Lengths (Å) of Key Configurations in the $[FeFe]_P$, $H[FeFe]_P$, and $HH[FeFe]_P$ Intermediates of the Cycle in Vacuo, cf. Figure 4

	Fe_p-Fe_d	$N-Fe_{surf1}$	Fe_d-H	Fe_p-S_{surf}	Fe_p-C of $(\mu\text{-}(CN)_p)$	Fe_d-C of $(\mu\text{-}(CN)_d)$
$[FeFe]_P$	2.48	1.96		2.28	1.95	1.84
$[FeFe]_P^{-1}$	2.49	2.01		2.27	1.99	1.85
$H[FeFe]_P$	2.51	2.02	1.52	2.35	1.92	1.98
$H[FeFe]_P^{-1}$	2.53	2.02	1.52	2.38	1.91	2.01
$HH[FeFe]_P$	2.78	2.04	1.68, 1.69	2.32	1.89	2.07
$HH[FeFe]_P^{-1}$	3.05	2.05	1.69, 1.71	2.21	1.94	2.02

In the enzyme, the diiron cluster is bridged by a dithiol chelating group. Here, we completed the formation of $[FeFe]_P$ by replacing the S atom of the dithiol bridge further from the surface, S_{chel}, with a hydrogenated phosphorus, PH, to prevent breakage of the Fe_p-S_{chel} bond upon hydrogenation of S_{chel}, which would have a negative impact on the catalytic activity.[31] The ability of the P atom to retain four bonds in this environment opens a further degree of freedom. The H atom connected to the P could be replaced by any organic group (R) which could be used to tune the properties of the catalyst and the synthetic pathway. Neutral $[FeFe]_P$ linked as described to the pyrite surface and optimized in vacuo is stable with "V-up" on Fe_d, cf. Figure 3.

The modified diiron cluster occupies roughly half of the surface of the simulation cell used here. The surface is thus densely functionalized, cf. Figure 3b. The distance of closest approach between the cluster replicas is 3.35 Å, that between the H atoms of the $(CN)_d$ of one cluster and of the $(CN)_p$ of its neighbor. The use of this simulation cell allows studying H_2 formation at high coverage within an affordable computation time.

Water Environment. The water environment was modeled using 79 water molecules, either without an extra proton ("neutral water") or with one ("acidified water"). Excluding the volume of the slab, estimated from the pyrite bulk density, and that of the cluster determined from tabulated van der Waals radii, the density of the 79 H_2O molecules within our simulation cell is close to the density of water at standard conditions. Our explicit quantum treatment of the water molecules not only takes into account the electrostatic effects but also provides a description of proton diffusion in water[57] and of proton sharing between the cluster and water. As demonstrated previously,[30] both these aspects are important for a more realistic representation of the system and its dynamics.

4. H_2 Production by the Supported Catalyst. In this section, we report studies of the pathway for hydrogen production by the $[FeFe]_P$ cluster via static calculations in vacuo (section 4.1) and finite temperature FPMD simulations in water (section 4.2).

4.1. Production of H_2 in Vacuo. In our previous studies[29,30] of the $[FeFe]_H$ cluster of Figure 2a, H_2 production occurred by two sequential reductions and protonations of the distal iron. We have carried out analogous studies of the $[FeFe]_P$ cluster bound to the surface. The bond lengths of the configurations optimized during the production cycle are reported in Table 1.

4.1.1. Initial Configuration. The structure of the starting neutral configuration is shown in Figures 3 and 4a. The supported catalyst has an odd number of electrons when neutral. We found that the unpaired spin is localized mainly on Fe_{surf1} (75%) and Fe_d (22%). These percentages are obtained by projecting the Kohn−Sham (KS) orbitals onto atomic wave functions. (See the Supporting Information for plots of the spin density.) Fe_p and Fe_d have projected charges of $-0.65e$ and $-0.66e$, respectively (where $e = 1.6 \times 10^{-19}$ C is the proton charge). If, despite the net spin on Fe_d, one supposes, in accord with the conventional view,[4,13] that both iron atoms are in the Fe(II) oxidation state, these projected charges imply that the 6 (5) ligands on Fe_p (Fe_d) contribute $-2.65e$ ($-2.66e$), with an average contribution of $-0.44e$ ($-0.53e$) per ligand. As electrons and protons are added during the course of the cycle, the projected charges and excess spins of course change. The relevant charges and electron number changes during the cycle are listed in Table 2. The HOMO−LUMO gap is 0.16 eV.

Table 2. Relevant Charges (in Units of the Proton Charge $e = 1.6 \times 10^{-19}$ C) and Electron-Number Changes in the $[FeFe]_P$, $H[FeFe]_P$, and $HH[FeFe]_P$ Intermediates of the Cycle in Vacuo, cf. Figure 4[a]

	change of electron number		charge			
	ΔN_{slab}	$\Delta N_{cluster}$	Fe_p	Fe_d	first H	second H
$[FeFe]_P$, Figure 4a			−0.66	−0.65		
$[FeFe]_P^{-1}$, Figure 4e	+0.61	+0.35	−0.67	−0.68		
$H[FeFe]_P$, Figure 4b	−0.38	+0.39	−0.66	−0.70	0.04	
$H[FeFe]_P^{-1}$, Figure 4f	+0.74	+0.20	−0.66	−0.71	0.03	
$HH[FeFe]_P$, Figure 4c	−0.72	+0.76	−0.65	−0.60	0.12	0.11
$HH[FeFe]_P^{-1}$, Figure 4g	+0.39	+0.59	−0.72	−0.63	0.11	0.09

[a] ΔN_{slab} ($\Delta N_{cluster}$) is the difference in electron number between adjacent configurations in the path, following the order of the table. The charges have been estimated by projection of the Kohn−Sham orbitals onto atomic wavefunctions. On order of 1% of the added electron charge is not accounted for by the projection.

4.1.2. One-Electron Reduction of $[FeFe]_P$. After addition of one electron to the system, the total number of electrons is even, the system charge is −1, and there is no net spin. The extra electron fills the valence band of the pyrite, and the HOMO−LUMO gap is 0.37 eV. About two-thirds of the extra charge is delocalized within the slab, and one-third goes into the cluster. The latter contributes a small increment of electron charge to Fe_d (4%), while the remainder goes to the most electronegative atoms linked to Fe_d: the O atoms of the CO groups and the P atom. In other words, that fraction of the added charge which resides in the cluster is localized on Fe_d and its most electronegative ligands. In this generalized sense, Fe_d is partly reduced. The optimized geometry is shown in Figure 4e.

4.1.3. Protonation of $[FeFe]_P^{-1}$. Adding a proton to Fe_d, cf. Figure 4b, forms the neutral system $H[FeFe]_P$. The hydrogen affinity is 372.5 kcal/mol, the total energy change after adding separately both the electron and the proton. The spin density remains zero, but the charge distribution changes significantly. The electron charge on the added proton is 0.95, implying that it is a hydrogen atom that is actually bound to Fe_d. This charge comes partly (about 38%) from the FeS_2 surface, and the rest from the cluster, primarily from the electronegative O and P atoms ligated to Fe_d which had increased their electron number significantly in the previous step. The HOMO−LUMO gap is 0.40 eV. The HOMO and LUMO, however, are localized primarily within the slab.

4.1.4. Reduction of $H[FeFe]_P$. Upon addition of a second electron to the system to form $H[FeFe]_P^{-1}$, about three-quarters of the charge goes into the slab and only one-quarter into the cluster, as expected from the LUMO of $H[FeFe]_P$. The spin of this odd-electron system is localized on two iron atoms in the slab, cf. the Supporting Information. The HOMO−LUMO

(57) Marx, D.; Tuckerman, M. E.; Hutter, J.; Parrinello, M. *Nature* **1999**, *397*, 601–604.

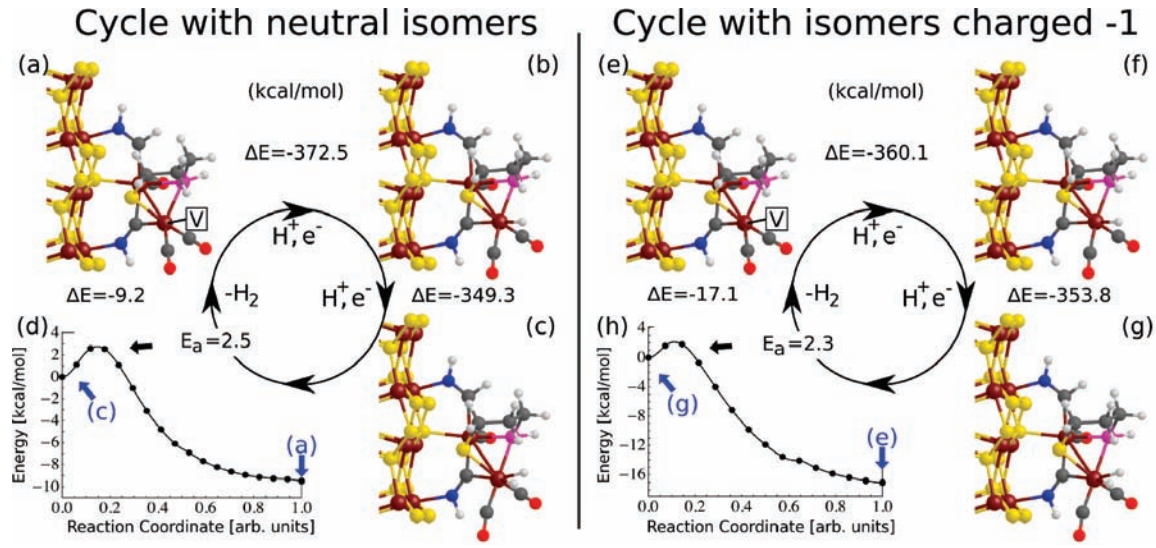

Figure 4. Catalytic cycles in vacuo for H_2 production by the $[FeFe]_P$ catalyst; (a)−(d), neutral isomers, (e)−(h) isomers charged −1. (a) Starting configuration with a vacant site on Fe_d. (b) The first H atom has been added to Fe_d. (c) The second H atom has been added to Fe_d. ΔE indicates the energy change (in kcal/mol), and (d) E_a is the energy barrier encountered during desorption of a H_2 molecule from (c) to (a) along the minimum energy path computed via the string method at $T = 0$. The continuous black line represents a cubic interpolation. Similarly for (e)−(h). The color code is that of Figure 3.

energy gap is now 0.14 eV. The optimized geometry is shown in Figure 4f.

4.1.5. Protonation of $H[FeFe]_P^{-1}$. We added a proton to $H[FeFe]_P^{-1}$ on Fe_d to form $HH[FeFe]_P$. This system is neutral, and the location of the spin changes mainly to Fe_p (51%) and Fe_d (38%). The hydrogen affinity of $H[FeFe]_P$ is 349.3 kcal/mol. The additional proton on Fe_d in $HH[FeFe]_P$ modifies the electron charge density of $H[FeFe]_P^{-1}$ by taking on 0.89 electrons. 0.74 comes from the surface, and the remainder comes from Fe_d and the first H, cf. Table 2. The HOMO−LUMO gap is 0.28 eV. The H−H distance between the two H atoms on Fe_d is 0.839 Å; the two Fe_d−H bond lengths are 1.683 and 1.695 Å. The optimized structure is shown in Figure 4c. The energy barrier for H_2 desorption from the neutral cluster, computed using the string method, is 2.5 kcal/mol, cf. Figure 4d. The desorption is exothermic: the energy of the free H_2 plus $[FeFe]_P$, Figure 4a, is lower by 9.2 kcal/mol than that of $HH[FeFe]_P$.

4.1.6. Reduction of $HH[FeFe]_P$. Adding a further electron to the system before H_2 desorption forms $HH[FeFe]_P^{-1}$, cf. Figure 4g. H_2 remains bound to Fe_d. About 40% of the extra charge goes into the slab and 60% into the cluster. There is no spin polarization, and the HOMO−LUMO gap is 0.36 eV. The H−H distance between the two H atoms on Fe_d reduces slightly to 0.835 Å; the two Fe_d−H bond lengths are 1.694 and 1.713 Å. The computed energy barrier for H_2 desorption is now 2.3 kcal/mol, cf. Figure 4h, an unimportant reduction with respect to the barrier in section 4.1.5. The desorption is exothermic, and the energy of the free H_2 plus $[FeFe]_P^{-1}$, Figure 4e, cluster is lower by 17.1 kcal/mol than that of $HH[FeFe]_P^{-1}$.

4.2. Production of H_2 from Water. To investigate the catalytic cycle for H_2 production from acidified water, we examined whether successive capture of protons added to the water in the simulation cell can occur and result in H_2 release. We started by equilibrating the $[FeFe]_P^{-1}$ catalyst in neutral water at 300 K for 3 ps. We analyzed several configurations extracted from the simulation by computing the KS orbitals and by projecting them onto atomic wave functions as described in section 4.1. The HOMO−LUMO energy gaps in these configurations are in the range 0.36−0.44 eV, and both the HOMO and the LUMO are almost entirely (90−95%) delocalized within the slab.

4.2.1. First Protonation of Fe_d. After the equilibration described above, we added one proton to the water molecule closest to Fe_d. One picosecond later, we increased the temperature to 330 K, and after 2 ps the proton diffused away into the water via the Grotthuss-shuttle mechanism.[57] As observed in our previous study,[30] the transfer of a proton from the water to Fe_d does not occur spontaneously within a few picoseconds, indicating that the process is activated.

To increase the probability of observing proton transfer to Fe_d, we reduced the spatial region accessible to the proton by constraining the O−H bond lengths of three water molecules close to Fe_d. The proton was confined to a group of seven water molecules. During a simulation lasting 0.95 ps at $T = 300$ K, we observed that the proton spent most of the time shuttling between the two molecule closest to Fe_d. We then removed the constraints and increased the temperature to 330 K. During the remaining 3.6 ps of the simulation, the proton remained relatively close to Fe_d (less than 6 Å). A snapshot from the simulation is shown in Figure 5a. Even though the H^+ was relatively near Fe_d, proton transfer to Fe_d did not occur, confirming that there is a free energy barrier to the transfer. We then estimated the barrier to Fe_d protonation by thermodynamic integration in a constrained FPMD simulation at $T =$ 330 K (the temperature at which all the FPMD simulations presented in the following were carried out). However, estimation of the barrier by thermodynamic integration is difficult because it requires simulating a quasi-static transformation by slow variation of the reaction coordinate, which is limited by available computational resources. Too rapid speed and inadequate choice of reaction coordinate lead to dissipation which in turn causes overestimation of the barrier.

To compute the free energy barrier we started from the configuration of Figure 5a,b. We used the reaction coordinate proposed by Leung et al. in ref 44. This reaction coordinate is a linear combination of the three O−H bond lengths of an H_3O^+. We denote those distances as R1, R2, and R3 and define the reaction coordinate R as R = R1−R2−R3. In an isolated hydronium ion the O−H bond lengths are 0.99 Å, so R is about −1.0 Å. Increase of R induces elongation of R1, preventing the elongation of R2 and R3, which fluctuate around their

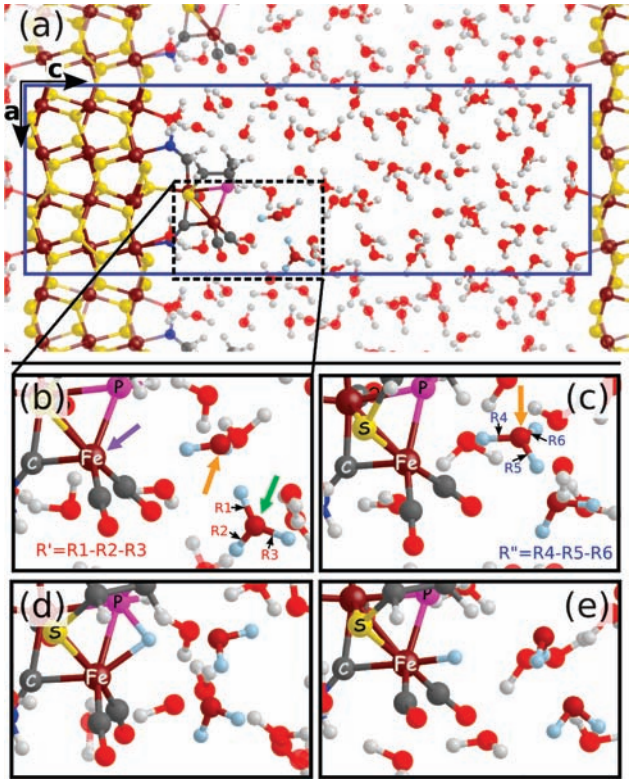

Figure 5. Protonation of Fe_d in water with an extra proton via constrained MD. The total charge of the system is zero. Panels (a)−(e) correspond to snapshots of a constrained FPMD trajectory at $T = 330$ K. (a) Starting configuration with a vacant site on Fe_d and a hydronium ion nearby. The simulation box is bounded by a blue solid line. The O and H atoms involved in the proton transfer are indicated with darker red and light blue balls, respectively. The color code for the remaining atoms is that of Figure 3. (b) Enlarged view of the reactive region indicated by a dotted box in (a). The purple and the green arrows indicate Fe_d and the hydronium ion. The orange arrow indicates a water molecule bridging the H_3O^+ and Fe_d. R1, R2, and R3 are the O−H bond lengths of the hydronium. $R' = R1-R2-R3$ is the reaction coordinate used to transfer one proton from the O-atom indicated with the green arrow to that indicated with the orange arrow. (c) The final configuration obtained varying continuously R′ from −1.05 Å to −0.65 Å. $R'' = R4-R5-R6$, with R4, R5, and R6 the O−H bond lengths of the hydronium indicated by the orange arrow, is the reaction coordinate for the transfer of the proton to Fe_d. (d) The final configuration with Fe_d-H obtained varying R″ continuously from −1.03 to −0.07 Å starting with the configuration of panel (c). (e) The configuration with Fe_d-H obtained removing the constraint R″ starting with the configuration of panel (d).

equilibrium values. This prevents proton escape by controlling R2 and R3 and allows selecting the proton that is transferred. As the O atom of the hydronium is 5.2 Å away from Fe_d and there is a water molecule between it and Fe_d, the transfer of the proton to Fe_d from the configuration of Figure 5a,b is a two-step process. First, a proton has to be transferred to the H_2O closest to Fe_d (indicated by an orange arrow in Figure 5b), and next, the proton is transferred from this molecule to Fe_d. For each step, we used a different coordinate. R′ is used for the first step and R″ for the second, as shown in Figure 5b,c, respectively.

Starting from the configuration of Figure 5b, we induced proton transfer to the water molecule closest to Fe_d by varying R′ at constant speed from −1.05 to −0.65 Å during an FPMD simulation lasting 1.2 ps. The resulting configuration is shown in Figure 5c. We estimated the free energy difference (ΔF) during the process by integrating the constraint-induced force on the reaction coordinate. We obtained ΔF=1.8 kcal/mol, corresponding to $\sim 3\ k_B T$ at $T = 330$ K. This is consistent with

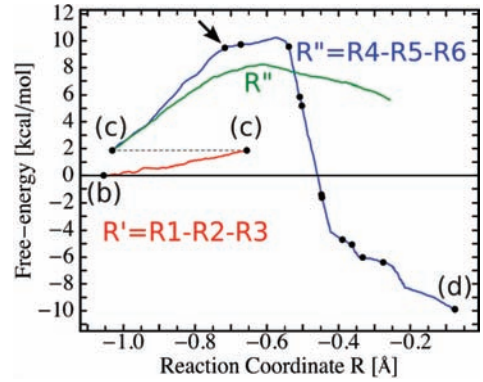

Figure 6. Free energy profile obtained by thermodynamic integration of the two reaction coordinates R′ (red solid line) and R″ (blue and green solid lines). The labels (b), (c), and (d) refer to the geometries of Figure 5b−d, respectively. The solid red line corresponds to the free energy for transferring a proton from the configuration of Figure 5b to that of Figure 5c, using R′ as the reaction coordinate. The target value of the constraint has been changed continuously in a simulation lasting 1.2 ps; see text. The solid blue line shows the free energy for transferring the proton to Fe_d, Figure 5d, obtained via thermodynamic integration of the reaction coordinates R″ varied continuously from −1.03 to −0.07 Å starting with the configuration of Figure 5c during a simulation lasting 10.7 ps. The black arrow indicates the point we changed the speed of R″. The simulation from (c) to the arrow lasted 1.4 ps, that from the arrow to (d) lasted 9.3 ps. The solid green line shows the free energy for transferring the proton to Fe_d obtained varying R″ with the speed used in the second part of the simulation associated to the solid blue line, in a simulation lasting 15.4 ps. The free-energy barrier to protonate Fe_d is 8.2 kcal/mol. The gray dotted line indicates the discontinuity due to the change of the reaction coordinate R′ to R″. The configurations of Figure 5b−d are indicated on the profile.

the observation that the proton shuttles between these two water molecules during the unconstrained FPMD simulation. The configuration of Figure 5c with a hydronium close to Fe_d does not correspond to a local minimum in the curves of Figure 6.

To transfer the proton from the hydronium to Fe_d, we used the reaction coordinate R″ defined in Figure 5c. We increased R″ from −1.03 to −0.26 Å during a simulation lasting 15.4 ps. The resulting free energy profile is shown as the solid green line in Figure 6. We obtained from that profile a value of 8.2 kcal/mol as our best estimate of (an upper bound to) the barrier.

To assess the validity of that estimate, we tested its sensitivity to the speed of R″ by increasing R″ from −1.03 to −0.07 Å during a simulation lasting 10.7 ps. We obtained a value of the free energy barrier of 10.2 kcal/mol from the free energy profile shown as a solid blue line in Figure 6, a 25% increase in the barrier resulting from the increase in speed, which implies that 8.2 kcal/mol may not be the fully converged value. The discontinuity in the profile in Figure 6 arises from the change of the reaction coordinate. The resulting configuration at $R'' = -0.07$ Å is shown in Figure 5d. We then removed the constraint, and Fe_d protonated spontaneously, forming $H[FeFe]_P$, cf. Figure 5e. The reaction is exothermic, the free energy of the product is lower than that of the reactants by at least 9.2 kcal/mol.

As the proton is transferred to Fe_d, it acquires electronic charge from the cluster/electrode system, becoming a nearly neutral H atom (cf. section 4.1.3). At that point, the hydronium has been reduced to a water molecule. The hydronium lone pair that was originally hydrophobic becomes hydrophilic again,[58,59] attracting a water molecule from the surrounding water. It is

(58) Kudin, K. N.; Car, R. *J. Am. Chem. Soc.* **2008**, *130*, 3915–3919.
(59) Tuckerman, M. E.; Marx, D.; Parrinello, M. *Nature* **2002**, *417*, 925–929.

this slow process, involving a substantial reorganization of the water with a relaxation time of order 10 ps, that makes estimation of the free energy barrier difficult. While overall the process has strong similarity to Marcus electron transfer, the additional coordinated proton transfer slows the process down.

The HOMO−LUMO gap of a few configurations selected from the constrained FPMD spanning the range of R″ in Figure 6 is in the interval 0.31−0.49 eV, and the HOMO is localized on the surface. During the proton transfer the projected charge of Fe_d is nearly constant in the range −0.68 to −0.75*e*, whereas the reacting H^+ takes charge from the catalyst, its projected electron number increasing from about 0.6 to 0.86. For comparison, we find that the projected electron number on each H atom of an isolated H_3O^+ is 0.47.

4.2.2. Second Protonation of Fe_d and H_2 Production. We equilibrated the neutral system $H[FeFe]_P$ for 3.2 ps at $T = 330$ K. As the affinity of $H[FeFe]_P$ for a second proton depends on the electronic charge of the cluster/electrode system, we added one proton and two electrons to the system. The first electron localizes primarily on the electrode and the second primarily on Fe_p and Fe_d. The number of electrons is even, and there is no net spin. We found via the following protocol spontaneous capture of the proton, initially placed quite far away. The O atom of the resulting H_3O^+ was 6 Å from Fe_d. To prevent proton diffusion during equilibration, we constrained all the three O−H bond lengths of the hydronium. After 0.5 ps at $T = 330$ K we removed the constraints. We observed proton diffusion among five H_2O molecules, indicated with balls and sticks in Figure 7. After 0.64 ps there are two water molecules between the H_3O^+ and Fe_d-H, cf. Figure 7a. After 1.38 ps there is an H_3O^+ close to Fe_d, Figure 7b. The proton is transferred to Fe_d, Figure 7c, and the H_2 molecule desorbs spontaneously, cf. Figure 7d, restoring the vacant site on Fe_d in the $[FeFe]_P^{-1}$ configuration. A movie of this 1.64 ps FPMD simulation is in the SI.

On the other hand, when only one electron is added so that the neutral system $HH[FeFe]_P$ is not formed. A trajectory generated by the same protocol from initial conditions otherwise the same did not result in spontaneous capture of the proton.

5. Discussion and Conclusions

The goal of this work was to find an active new catalyst for electrocatalytic hydrogen production from acidified water, one composed of abundant elements. The original idea was to attach the active center of the diiron hydrogenases to the $FeS_2(100)$ surface, as sketched in Figure 1. To meet the requirements of compatibility with the substrate, of stability, and of catalytic activity listed in the introduction we had to modify the cluster, as reported in more detail elsewhere.[31] Here we have demonstrated that the resulting model (cf. Figure 3) produces hydrogen when immersed in acidified water and supplied with electrons. This conclusion followed from first-principles static calculations and molecular-dynamics simulations carried out with the cluster attached to a (100) pyrite slab in vacuo and in a water environment.

Three categories of modifications of the $[FeFe]_H$ cluster to form $[FeFe]_P$ were described briefly in section 3 and more fully in ref 31. The first consists of removal of the methylthiol of the models of refs 29 and 30 from Fe_p and protonation, hydrogenation, and/or rearrangement of the CO and CN ligands of Fe_p and Fe_d. This allowed stable, tridentate bonding of the $[FeFe]_H$ cluster to the $FeS_2(100)$ surface with the vacant coordination site V on Fe_d exposed to the water. Second, the apical group X

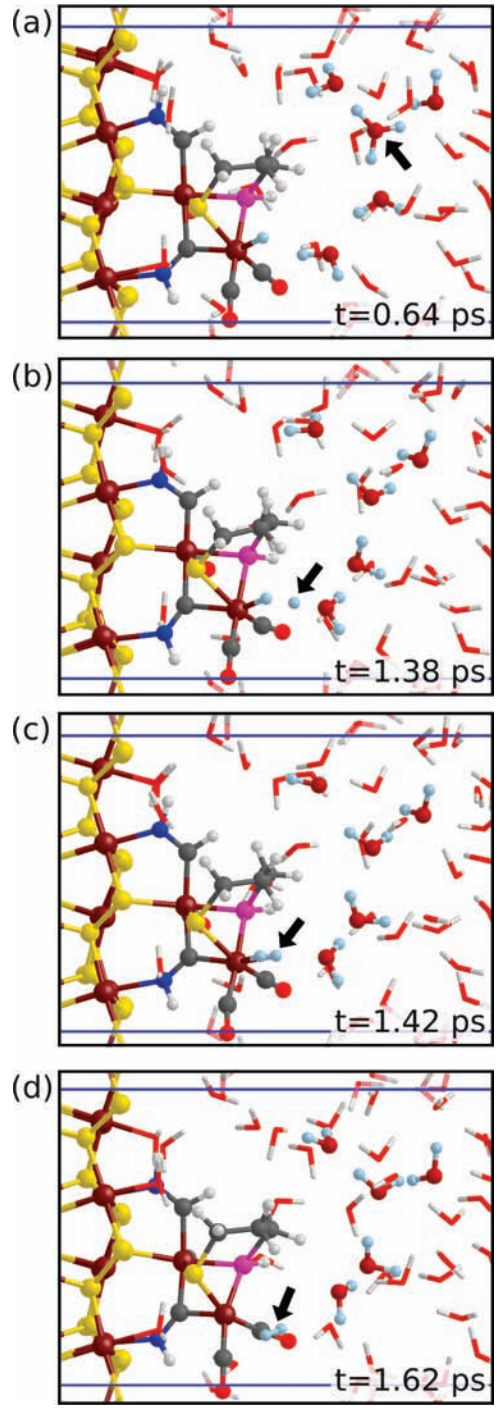

Figure 7. Set of snapshots from FPMD simulation of hydrogen production from the $H[FeFe]_P$ cluster at $T = 330$ K in water with an extra proton. There are two electrons added to the supported catalyst; the total charge of the system is −1. The elapsed time for each snapshot is shown in the panels. In the starting configuration, the hydronium (black arrow) is separated from Fe_d-H by two water molecules. We prevent proton diffusion by constraining the 3 O−H bonds of the hydronium for 0.64 ps; the resulting configuration is shown in (a). After 0.64 ps, we removed the constraints; the extra proton is shared between the water molecules depicted with balls and sticks. The O and H atoms of those molecules are indicated with darker red and light blue balls, respectively. The remaining water molecules are represented by sticks. The color code for the remaining atoms is that of Figure 3. The continuous blue line indicates the simulation box. (b) After 1.38 ps, the extra proton (black arrow) has migrated toward Fe_d-H. (c) The H_2 molecule (black arrow) has formed on Fe_d, followed (d) by spontaneous desorption of H_2 (black arrow), restoring the starting configuration of the cycle with a vacant site on Fe_d and a charge of −1.

of the chelating bridge was chosen as CH_2, forming a PDT bridge. Finally, that sulfur of the bridge which was exposed to the water was replaced by a PH group to stabilize the bridge and, ultimately, to allow fine-tuning of the catalyst by substituting for the H atom.

As found in our previous study,[30] transfer of the first proton from the water to Fe_d is the bottleneck of the catalytic cycle because of its competition with rapid proton diffusion via the Grotthuss-shuttle mechanism. Using thermodynamic integration, we found a free energy barrier of about 8.2 kcal/mol to transfer the proton from the water to Fe_d. This value should be considered an upper estimate for two reasons: first, we used a one-dimensional reaction coordinate that may neglect other degrees of freedom important to the process. Second, the speed of constraint variation should be slow enough to allow equilibration of the system, in particular of the water molecules. Computational cost imposed on us a lower bound on that speed which may have not been sufficient for full equilibration. An upper bound of 8.2 kcal/mol for proton transfer at 330 K, however, implies that the bottleneck is a mild one at room temperature and keeps open the possibility of a very high turnover number. From the plot of the free energy of Figure 6, we also find that the energy of system with a proton on Fe_d is lower by at least 9.2 kcal/mol than that with the proton in water and the vacancy on Fe_d. This implies that after the proton is transferred to Fe_d the configuration $H[FeFe]_P^{-1}$ should be stable long enough for a second protonation to occur. Indeed, we found that the second protonation of Fe_d occurs spontaneously in the short time spanned by our simulation. After the second protonation, an H_2 molecule forms and desorbs without evidence of an inhibiting energy barrier. In ref 30, we suggested that the hydride character of the H on Fe_d is the reason of the higher reactivity of Fe_d-H relative to that of Fe_d-V. However, here we found that the H atom on Fe_d is almost neutral, not a hydride. Instead, we have learnt that it is the difference in the microscopic configuration of the water environment of Fe_d which is key. In contrast to $[FeFe]_P^{-1}$, for $H[FeFe]_P^{-2}$ the closest water molecule persistently orients so that one of its hydrogen remains only between 1.3 and 2 Å away from the first H, which projects 1.5 Å from Fe_d into the water. There is a channel of hydrogen bonds for proton transfer to that close molecule from a relatively distant hydronium. When the extra proton arrives at the nearby H_2O, it is that closest H which transfers. As it moves inward, it draws electrons from Fe_d and the first H forming an incipient Fe_d-H_2 complex which rapidly dissociates, freeing the H_2.

It may be possible to reduce the barrier to first protonation of the $[FeFe]_P^{-1}$ or possibly the $[FeFe]_P^{-2}$ configuration by replacing the H of the PH group with a more electronegative group R. The electronegativity and geometry of R would have to be tuned so as to modify the water configuration near the vacant coordination site on Fe_d without seriously impeding electron transfer to the Fe_p and Fe_d atoms in forming the $H[FeFe]_P^{-2}$ configuration antecedent to the second protonation. The goal would be to approximate the favorable configuration found for $H[FeFe]_P^{-2}$ by bringing a water hydrogen near to the vacant coordination site of $[FeFe]_P^{-1}$ or possibly $[FeFe]_P^{-2}$.

In conclusion, we have presented FPMD simulations of hydrogen production by a coupled catalyst-electrode system consisting of a modified $[FeFe]_H$ cluster, $[FeFe]_P$, supported on an $FeS_2(100)$ surface in acidified water, a system far more complex than those typically treated by first-principles methods. The principal findings of the present paper are as follows: (i) the $[FeFe]_P$ cluster proposed in this paper is able to form a stable, tridentate link to the surface. (ii) In this configuration there is a vacant site on Fe_d in the "up" position able to accept protons from acidified water. (iii) There is a relatively low activation energy pathway for hydrogen production from acidified water, a mild bottleneck in the process being the first protonation of Fe_d. (iv) The second protonation is much faster, and there is no further barrier for H_2 desorption. To achieve these results, we have used first-principles molecular-dynamics simulations at an advanced level of system complexity.

Acknowledgment. This work was supported by the Department of Energy under Grant No. DE-FG02-06ER-46344. Princeton Tigress & NERSC computation facilities are acknowledged for CPU time.

Supporting Information Available: Electron spin density in the catalytic cycle in vacuo, complete ref,[34] and movie of hydrogen production in water. This material is available free of charge via the Internet at http://pubs.acs.org.

JA910694P